system is able to track step inputs at $d(1)$. [We note that with a zero r input (Fig. 2), the output $y_p(s)$ of the plant $P(s)$ is given by $-P(s)K(s)[I + P(s)K(s)]^{-1}d(s)$; thus, in the steady state, the component of $y_p(t)$ corresponding to $\phi(t)$ goes to -0.1 deg in response to the positive step input of 0.1 deg at $d(1)$.] We note that the effect of this input to the body rate is low, and the interactions between the rigid-body dynamics and the flexible dynamics are rather low; the rigid-body dynamics continue to influence the flexible body dynamics more than vice versa. This is evident from the response plots of the flexible mode shown in Fig. 4: the overall shape of these curves are similar to those of the rigid-body rate response curves.

We now design a controller using the loop shaping technique. After several iterations we choose the following weighting transfer functions: $W_1(s) = 1/(s+1)$ and $W_2(s) = I$. The order of the controller is, therefore, six. We note that the response of the closed-loop system to a step input of 0.1 deg at the ϕ channel is similar to that of the earlier design. We observe a little increase in the deflection of the flexible mode and its rate (not shown).

The effect of controller order reduction is evaluated next. In both cases, the order can be reduced to three with very little change in the robustness properties or the time-domain performance of the closed-loop system with reduced-order controllers. Moreover, a perturbation of 30% in the natural frequency and 15% in the coupling coefficients of the flexible modes is observed to have no effect on the robustness of the closed-loop system and the time-domain performance for the first design; a slight deterioration in the response of the flexible mode is observed. For brevity, the response plots are not included. Thus, the controllers obtained by the feedback configuration and the loop shaping technique have many common characteristics and yield similar closed-loop responses.

Conclusions

We presented different ways to build the generalized plant. We showed that the feedback configuration has certain advantages over the cascade configuration, which can usefully be employed while computing the $\mathcal{H}_\infty$ robust controller by the Glover–Doyle algorithm. By providing a feedback configuration interpretation of the McFarlane–Glover loop shaping technique, we conclude that it has characteristics similar to that of the feedback configuration. We then establish this by showing that the robust controllers designed to control the roll dynamics of a satellite with flexible appendages generates closed-loop systems that have similar robustness properties and time-domain performance.

References

[1]Glover, K., and Doyle, J. C., "State-Space Formulae for All Stabilizing Controllers that Satisfy an H_∞ Norm Bound and Relations to Risk Sensitivity," *Systems and Control Letters*, Vol. 11, No. 3, 1988, pp. 167–172.

[2]McFarlane, D. C., and Glover, K., *Robust Controller Design Using Normalized Coprime Factor Plant Descriptions*, Vol. 138, Lecture Notes in Control and Information Sciences, Springer–Verlag, Berlin, 1990, Chap. 6.

[3]Vidyasagar, M., *Control System Synthesis: A Factorization Approach*, MIT Press, Cambridge, MA, 1985, Chap. 6.

[4]McFarlane, D., Glover, K., and Vidyasagar, M., "Reduced-Order Controller Design Using Coprime Factor Model Reduction," *IEEE Transactions on Automatic Control*, Vol. 35, No. 3, 1990, pp. 369–373.

[5]Maciejowski, J. M., *Multivariable Feedback Design*, Addison–Wesley, Wokingham, England, UK, 1989, Chap. 6.

[6]George, K. K., "$\mathcal{H}_\infty$-Based Robust Controller for Aerospace Vehicles," Ph.D. Thesis, Dept. of Aerospace Engineering, Indian Inst. of Science, Bangalore, India, Nov. 1996.

[7]Safonov, M. G., Limebeer, D. J. N., and Chiang, R. Y., "Simplifying the H^∞ Theory via Loop-Shifting, Matrix-Pencil and Descriptor Concepts," *International Journal of Control*, Vol. 50, No. 6, 1989, pp. 2467–2488.

[8]Freudenberg, J. S., and Looze, D. P., *Frequency Domain Properties of Scalar and Multivariable Feedback Systems*, Vol. 104, Lecture Notes in Control and Information Sciences, Springer–Verlag, Berlin, 1988, Chap. 5.

Efficient, Near-Optimal Control Allocation

Wayne C. Durham*
Virginia Polytechnic Institute and State University, Blacksburg, Virginia 24061-0203

Introduction

WE address the problem of allocating several redundant control effectors in the generation of specified body-axis moments. The effectors are constrained by position limits and are assumed to be linear in their effectiveness. The optimal solution to this problem in terms of generating maximum attainable moments for admissible controls was previously addressed in Refs. 1–3. The computational complexity of the algorithm developed in Ref. 2 to obtain such solutions is proportional to the square of the number of controls, which could become problematic in real-time applications. Other methods that generate solutions for maximum attainable moments, e.g., null-space intersections,[4,5] are even more computationally complex. This Note describes a computationally simple and efficient method to obtain near-optimal solutions. The method is based on prior knowledge of the controls' effectiveness and limits and on precalculation of several generalized inverses based on those data.

Nature of the Problem

For m controls $\boldsymbol{u}$ with effectiveness B in producing moments $\boldsymbol{m}$, the allocation problem is an underdetermined system of linear equations $\boldsymbol{m} = B\boldsymbol{u}$ with admissible controls $\boldsymbol{u} \in \Omega$, $\Omega = \{\boldsymbol{u} \mid u_i \geq u_{i,\min}, u_i \leq u_{i,\max}\}$, $i = 1, \ldots, m$. The admissible controls map to the attainable moments Φ where $\Phi = \{\boldsymbol{m} \mid \boldsymbol{m} = B\boldsymbol{u}, \boldsymbol{u} \in \Omega\}$. The attainable moments in Φ are bounded by a polyhedron whose boundary consists of parallelograms (the facets), each associated with a pair of controls. The maximum attainable desired moment $\boldsymbol{m}_d$ in some arbitrary direction occurs at the intersection of a line in the same direction as $\boldsymbol{m}_d$ with a facet on the convex hull. The determination of the proper facet requires a search that terminates when the proper facet is found: There is no assurance that this will not be the last facet tested.

The reason for the requirement to search the facets is that there is no simple way to relate a direction in moment space to the four directions that define the vertices of a particular facet. As a result, the facets must be individually tested. There are several ways in which the search order may be prioritized that will reduce the average search time, but none of these methods ensure that the worst case (in which the correct facet is the last one examined) will not often occur. In real-time applications, the frequently occurring worst case may drive the timing budgeted for control allocation.

Approximating Φ

The ideal facets of Φ, if such existed, would be those for which simple tests could be applied to $\boldsymbol{m}_d$ to determine the facet toward which it points and for which a subsequent closed-form solution to the allocation problem existed. Therefore, we seek to approximate the polyhedron that is Φ with another polyhedron whose facets satisfy this ideal requirement. We begin by constructing such a polyhedron, then determine the closed-form solutions associated with its facets.

Sectors of Moment Space

The simplest tests are relational among and between the three components of $\boldsymbol{m}_d$. Each component may be tested for sign, and the relative magnitudes of the three components established. The sign of each of the three components serves to determine the orthant (a

Received June 29, 1998; revision received Sept. 3, 1998; accepted for publication Sept. 15, 1998.

*Associate Professor, Department of Aerospace and Ocean Engineering. Senior Member AIAA.

generalized quadrant) in which the desired moment lies, and the relative magnitudes further divide each orthant into six sectors. Thus, moment space may be divided into 48 sectors that are each bounded by three directions.

Define $\boldsymbol{m}_d^T = \{m_{d_1} \;\; m_{d_2} \;\; m_{d_3}\}$. Orthants are numbered from 0 to 7 by binary numbers formed from the signs of the components according to $\{-,-,-\} \Rightarrow$ number 0, $\{-,-,+\} \Rightarrow$ number 1, ..., $\{+,-,-\} \Rightarrow$ number 4, etc. Sectors within each orthant are arbitrarily numbered

$$1: \left|m_{d_1}\right| > \left|m_{d_2}\right| > \left|m_{d_3}\right|, \qquad 4: \left|m_{d_3}\right| > \left|m_{d_1}\right| > \left|m_{d_2}\right|$$

$$2: \left|m_{d_2}\right| > \left|m_{d_1}\right| > \left|m_{d_3}\right|, \qquad 5: \left|m_{d_2}\right| > \left|m_{d_3}\right| > \left|m_{d_1}\right|$$

$$3: \left|m_{d_1}\right| > \left|m_{d_3}\right| > \left|m_{d_2}\right|, \qquad 6: \left|m_{d_3}\right| > \left|m_{d_2}\right| > \left|m_{d_1}\right|$$

For example, a desired moment in the direction $\{1 \;\; -3 \;\; 2\}$ is in orthant 2, sector 5.

Within each orthant, each sector is an infinitely high triangular pyramid with its apex at the origin and three edges that are half-lines in moment space. In orthant 7 the three half-lines for each sector are in directions of

$$1: \begin{Bmatrix}1\\1\\1\end{Bmatrix}, \begin{Bmatrix}1\\1\\0\end{Bmatrix}, \begin{Bmatrix}1\\0\\0\end{Bmatrix}, \qquad 4: \begin{Bmatrix}1\\1\\1\end{Bmatrix}, \begin{Bmatrix}1\\0\\1\end{Bmatrix}, \begin{Bmatrix}0\\0\\1\end{Bmatrix}$$

$$2: \begin{Bmatrix}1\\1\\1\end{Bmatrix}, \begin{Bmatrix}1\\1\\0\end{Bmatrix}, \begin{Bmatrix}0\\1\\0\end{Bmatrix}, \qquad 5: \begin{Bmatrix}1\\1\\1\end{Bmatrix}, \begin{Bmatrix}0\\1\\1\end{Bmatrix}, \begin{Bmatrix}0\\1\\0\end{Bmatrix}$$

$$3: \begin{Bmatrix}1\\1\\1\end{Bmatrix}, \begin{Bmatrix}1\\0\\1\end{Bmatrix}, \begin{Bmatrix}1\\0\\0\end{Bmatrix}, \qquad 6: \begin{Bmatrix}1\\1\\1\end{Bmatrix}, \begin{Bmatrix}0\\1\\1\end{Bmatrix}, \begin{Bmatrix}0\\0\\1\end{Bmatrix}$$

The vectors for the sectors of the other seven orthants are similar, except the signs of the components of each direction must be changed to place the vectors in the appropriate orthant. Neglecting duplications between adjacent sectors, there are 26 directions used to define the 48 sectors.

These sectors can be used to approximate the attainable moment subset Φ. The intersection of each of the three half-lines of each sector with the boundary of Φ is calculated. Connecting these three points defines a base for the triangular pyramid in a given sector. The 48 pyramids thus defined are collectively an approximation to Φ. (Note that, if Φ were a sphere, the polyhedron generated by this method would be a hexakisoctahedron.) The pyramid in which a given half-line lies and toward whose base it points is easily established by the signs and relative magnitudes of the components of a vector in that direction. The bases of the triangular pyramids, therefore, satisfy the first half of our requirements for ideal facets.

Closed-Form Solutions Within Sectors

In Ref. 1, we described a technique for tailoring a generalized inverse to fit exactly the attainable moment subset Φ at a certain number of points on the boundary of Φ; for the three-moment problem this number is three. Tailored generalized inverses have long been considered a curiosity with no practical importance in solving the general problem. In the context of the sectors defined earlier they are, however, a perfect source of closed-form solutions. For each sector a tailored generalized inverse may be calculated that yields the unique solutions exactly at the three points of intersection with the boundary of Φ. The portion of Φ for which the generalized inverse provides admissible solutions is convex and contains the origin. Therefore, the generalized inverse will provide admissible solutions everywhere within the pyramid associated with the sector. (It is true that each generalized inverse provides admissible solutions in other sectors, possibly even improving on the generalized inverse associated with another sector at some points, but there are no simple rules for determining when it should be used there.) The technique for determining tailored generalized inverses for the three-moment problem is more fully addressed in Ref. 5. In summary, the procedure is as follows:

1) Select the three directions that define the sector.

2) Using any desired method, e.g., direct allocation, determine the controls $\boldsymbol{u}_1^*$, $\boldsymbol{u}_2^*$, and $\boldsymbol{u}_3^*$ and moments $\boldsymbol{m}_1^*$, $\boldsymbol{m}_2^*$, and $\boldsymbol{m}_3^*$ at the intersection of the three directions with the boundary of Φ.

3) Form the matrices M, $M^T = [\boldsymbol{m}_1^* \;\; \boldsymbol{m}_2^* \;\; \boldsymbol{m}_3^*]$ (moments are rows of M, a 3×3 matrix), and U, $U^T = [\boldsymbol{u}_1^* \;\; \boldsymbol{u}_2^* \;\; \boldsymbol{u}_3^*]$ (controls are rows of U, a $3 \times m$ matrix).

4) Partition B into $B = [B_1 \;\; B_2]$, where B_1 is square and invertible, and similarly U into $U = [U_1 \;\; U_2]$.

5) Calculate P_2 from $P_2^T = M^{-1}U_2$.

6) Calculate $P_1 = B_1^{-1} - B_1^{-1}B_2P_2$.

7) Assemble P from $P^T = [P_1^T \;\; P_2^T]$.

Improving the Approximation

In aircraft control applications the attainable moment subset Φ tends to have different ranges of values along each of its three axes. In particular, they are elongated along the pitching moment axis and asymmetrical along that axis as well. The asymmetry in pitching moments is due to the asymmetry in positive and negative deflection limits of pitching moment surfaces such as the horizontal tail, which results from the definition of zero deflection. The effect of disproportionate ranges and asymmetries is to make the simple orthant–sector division of moment space a poor approximation to the attainable moment subset. Figure 1 shows the application of such a division on the example problem introduced in Ref. 2. In that example, the horizontal tail limits were from -24.0 to $+10.5$ deg, and the trailing-edge flap limits were from -8.0 to $+24.0$ deg. In Fig. 1a the entire attainable moment subset is shown. In Fig. 1b the wireframe outlines the attainable moment subset, and within the solid figure are moments attainable using the 48 generalized inverses with admissible controls. The volume so generated is 40.5% that of the entire volume of Φ.

The effect of the differences in the three dimensions of the three axes may be eliminated by transformations of the sector vectors in moment space. Thus, we consider sectors defined by $T\boldsymbol{v}_{i,j,k}$ for each vector k of each sector j in each orthant i. If a desired moment $\boldsymbol{m}_d$ lies within a transformed sector, then the vector $T^{-1}\boldsymbol{m}_d$ lies within the untransformed sector. We, therefore, seek T such that the collective volume of the transformed sectors is greatest. As before, each transformed sector will have a tailored generalized inverse associated with it. We then determine the orthant and sector of $T^{-1}\boldsymbol{m}_d$ using the usual relational tests and apply the appropriate generalized inverse to $\boldsymbol{m}_d$ to determine the controls.

A simple and reasonable first guess for T is a diagonal matrix T_{diagonal} with elements in the same ratio as those of the ranges of attainable values along each axis. For the example problem, this ratio is $C_l : C_m : C_n = 2.48 : 8.60 : 1.00$. Figure 2 shows the effect

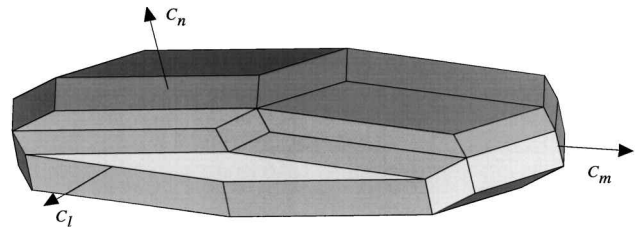

Fig. 1a Simple orthant–sector division: attainable moments.

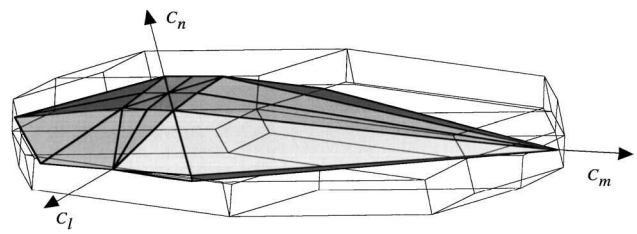

Fig. 1b Simple orthant–sector division: orthant-sectors within wireframe.

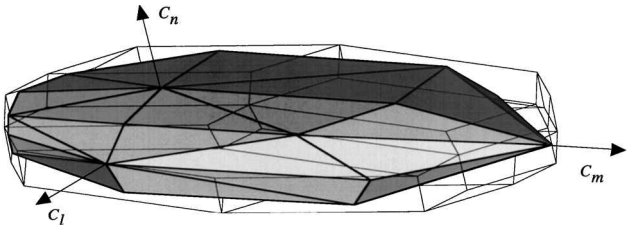

Fig. 2 Division with diagonal transformation.

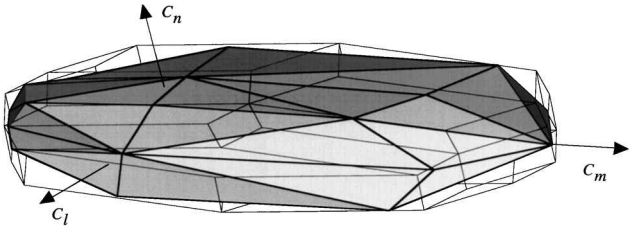

Fig. 3 Division with optimal transformation.

of transforming the sectors with these values. Here the volume of the approximation is 71.1% of maximum. In a linear sense this is not too bad; if the volumes were spheres the smaller would have a radius 89% that of the larger.

With some extra effort a better diagonal transformation matrix may be found. A cost function was formulated as

$$1 - \sum_{i=1}^{48} \frac{\text{vol}_i}{\text{vol}_{\max}}$$

in which vol_i is the volume of the ith sector. The first two diagonal elements of T (element 3, 3 was set to 1.00) were varied in a simplex algorithm borrowed from Ref. 6 to minimize the cost function. With termination criterion of $1.0e-8$ the transformation matrix was $T_{\text{diagonal}} = \text{diag}\{2.82 \;\; 12.3 \;\; 1.00\}$ and yielded a volume 74.6% of the maximum (linear, 91.0%). The figure that results is indistinguishable from that in Fig. 2 and is omitted.

The next logical step is to minimize the cost function using all nine elements of T. Again using the simplex algorithm with termination criterion of $1.0e-8$, this resulted in

$$T_{\text{global}} = \begin{bmatrix} 2.08 & -1.34e-4 & -0.672 \\ 0.346 & 9.68 & 0.271 \\ 0.212 & 2.12e-3 & 1.08 \end{bmatrix}$$

The resulting volume was 77.3% (linear, 92.0%). Figure 3 shows the polyhedron defined by this transformation. Again, there is not much difference between this and Fig. 2, except for a slight shifting around of uncovered volumes.

In many cases the position defined as zero deflection of a control is arbitrary. If so, then it is possible to redefine the control limits such that they are symmetric about the zero position. Application of symmetric control limits resulted in a much larger polyhedral approximation. The limits of the horizontal tails were redefined to ±17.25 deg and of the trailing-edge flaps to ±16.0 deg. The results for the case with no transformation were improved from 40.5 to 46.0%, with the optimal diagonal transformation matrix from 74.6 to 83.6% (with $T_{\text{diagonal}} = \text{diag}\{3.30 \;\; 8.86 \;\; 1.00\}$), and with the optimal global transformation matrix from 77.3 to 84.6% (linear, 94.6%). The results of the global transformation are shown in Fig. 4 with the transformation

$$T_{\text{global}} = \begin{bmatrix} 3.29 & 8.33e-4 & -3.68e-2 \\ 1.11e-1 & 8.94 & -3.95e-2 \\ -1.25e-1 & -1.31e-2 & 8.84e-1 \end{bmatrix}$$

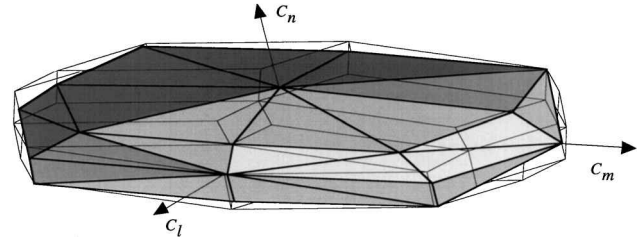

Fig. 4 Division with optimal transformation, symmetric control limits.

Algorithm Efficiency and Suboptimality

The algorithm presented represents a tradeoff between efficiency and optimality. Efficiency in this sense is execution time relative to other allocation methods, which is proportional to the number of floating-point operations required to determine a solution. The data storage requirements for a given method may also be of concern, but is not considered here. Optimality is measured by the extent to which the algorithm yields admissible solutions in response to demands that are theoretically attainable, i.e., the relative volume of Φ that the algorithm actually attains.

The use of a single (precomputed) generalized inverse P to generate solutions $\boldsymbol{u} = P\boldsymbol{m}_d$ requires $5m$ floating-point operations (three multiplications and two additions for each of m controls), which is very efficient. On the other hand, generalized inverses are far from optimal solutions: In the example problem, the minimum-norm solution (pseudoinverse) attains 34.5% by volume of Φ, whereas the largest (by volume) generalized inverse attains just over 55% of the attainable moments.

Direct allocation by design attains 100% of Φ. The number of floating-point operations required by direct allocation is difficult to predict for the general case, but it is known for the worst case. Assuming a complete description of the geometry of the attainable moment subset has been precomputed, for a given $\boldsymbol{m}_d$ the facets of Φ must be searched for the one yielding an admissible solution. Each test requires the multiplication of $\boldsymbol{m}_d$ by a (precomputed) 3×3 matrix, or 15 floating-point operations. The number of facets is $m(m-1)$, and in the worst case all facets will be tested. The final step in direct allocation requires scaling the results of the test, yielding a total of $15m(m-1) + m$ floating-point operations.

The polyhedral approximations described replace the tests required by direct allocation to sign and magnitude comparisons of the elements of $\boldsymbol{m}_d$, which require no floating-point operations. The test identifies one of the precomputed generalized inverses, and as before this requires $5m$ floating-point operations to determine the controls. The optimality of the solution may be greatly improved over the use of a single generalized inverse (from 55 to 84% by volume of Φ) without increasing the number of floating-point operations required for solution.

Conclusions

We have shown how polyhedral approximations to the attainable moment subset can be constructed. The volumetric sectors of the polyhedrons are each characterized by simple relations among the signs and relative magnitudes of vectors within them. Each volumetric sector is associated with a closed-form (generalized inverse) solution to the allocation problem that yields optimal (maximum) solutions at three points and suboptimal solutions in other directions. The polyhedral approximation requires that the solutions be precomputed, thus rendering it impractical for applications in which control effectiveness and limits are determined or estimated on the fly. The approximation has computational requirements on a par with those of single generalized inverses, but it may yield solutions that are much more nearly optimal.

Acknowledgment

This work was conducted under NASA Research Grant NAG 1-1449, supervised by John V. Foster of the NASA Langley Research Center.

References

[1]Durham, W. C., "Constrained Control Allocation," *Journal of Guidance, Control, and Dynamics*, Vol. 16, No. 4, 1993, pp. 717–725.

[2]Durham, W. C., "Constrained Control Allocation: Three-Moment Problem," *Journal of Guidance, Control, and Dynamics*, Vol. 17, No. 2, 1994, pp. 330–336.

[3]Durham, W. C., "Attainable Moments for the Constrained Control Allocation Problem," *Journal of Guidance, Control, and Dynamics*, Vol. 17, No. 6, 1994, pp. 1371–1373.

[4]Bordignon, K. A., and Durham, W. C., "Closed-Form Solutions to Constrained Control Allocation Problem," *Journal of Guidance, Control, and Dynamics*, Vol. 18, No. 5, 1995, pp. 1000–1007.

[5]Bordignon, K. A., "Constrained Control Allocation for Systems with Redundant Control Effectors," Ph.D. Thesis, Dept. of Aerospace and Ocean Engineering, Virginia Polytechnic Inst. and State Univ., Blacksburg, VA, Dec. 1996.

[6]Stevens, B. L., and Lewis, F. L., *Aircraft Control and Simulation*, 1st ed., Wiley, 1992, pp. 597, 598.

Does the Phugoid Frequency Depend on Speed?

S. Pradeep*
Indian Institute of Science, Bangalore 560 012, India
and
S. Kamesh†
Aeronautical Development Agency, Bangalore 560 017, India

Introduction

THE phugoid frequency is thought to be inversely proportional to the forward speed, although this has never been proved. Three counterexamples to this conviction are presented. Subsequently, it is shown that if the speed alone is varied, keeping the aerodynamic and thrust derivatives fixed by some means, the phugoid frequency remains unchanged, establishing that the phugoid frequency is independent of speed. The widespread belief of the dependency of the phugoid frequency on speed perhaps results from the fact that, in most instances, the aerodynamic derivatives vary with speed in such a manner as to make the phugoid time period roughly proportional to the speed.

The notation of Roskam[1] is used. The thrust derivatives are assumed to be combined with the aerodynamic derivatives; i.e., X_u stands for $X_u + X_{Tu}$, M_u stands for $M_u + M_{Tu}$, and M_α stands for $M_\alpha + M_{T\alpha}$.

Analysis

The earliest approximation to the phugoid mode was put forth by Lanchester,[2] who derived the following expression for phugoid frequency:

$$\omega_p = g\sqrt{2}/U_1 \tag{1}$$

This simple result suggests the following:

Conjecture A. The phugoid frequency is inversely proportional to the forward speed.

Data from flight tests are often in harmony with Conjecture A. In the absence of more accurate theory, it is widely believed that Conjecture A is true. This is stated in almost every text on atmospheric flight dynamics, often substantiated with a numerical example or two.

Received Dec. 1, 1997; revision received Nov. 13, 1998; accepted for publication Nov. 18, 1998.

*Assistant Professor, Department of Aerospace Engineering. Member AIAA.

†Scientist.

Table 1 Counterexamples to Conjecture A

Aircraft	Page no. in Ref. 3	Altitude	Mach number	ω_p, rad/s
F-104	51	Sea level	0.257	0.1520
			0.800	0.0504
			1.100	0.0523
		35,000 ft	0.600	0.0709
			0.900	0.0839
Convair 880 A	202	35,000 ft	0.700	0.0528
			0.800	0.0538
			0.860	0.0504

At the outset, counterexamples to this conjecture are shown. Consider the data in Table 1 from Heffley and Jewell.[3]

The phugoid frequency increases with increase in forward speed, disproving Conjecture A, in three instances in Table 1: when the mach number increases from 0.8 to 1.1 at sea level for the F-104, when the mach number increases from 0.6 to 0.9 at 35,000 ft for the F-104, and when the mach number increases from 0.7 to 0.8 at 35,000 ft for the Convair 880M. These results call for a reexamination of the age-old statement in Conjecture A.

Consider the following expression for phugoid frequency, proposed by the authors in a recent study:[4]

$$\omega_p = \sqrt{\frac{g(M_\alpha Z_u - M_u Z_\alpha)}{M_q Z_\alpha - U_1 M_\alpha}} \tag{2}$$

In Ref. 4, numerical simulations involving 15 cases of various types of aircraft under varying flight conditions were carried out to verify the authenticity of this expression. The data were taken from Appendix C of Roskam's text on flight dynamics.[1] This collection of data pertains to six modern aircraft in a total of 16 flight conditions. The aircraft chosen represent diverse missions: a small four-place transportation airplane, a 19-passenger commuter airliner, a small jet trainer, a medium-size high-performance business jet, a supersonic fighter-bomber, and a large wide-body jet transport. The flight conditions range from power approach at sea level to cruise at medium and high altitudes. The database is thus representative of a wide spectrum of airplanes and flight conditions.

It was shown that the approximate expression (2) does not differ from the exact value by more than 4% in the 15 cases considered. The corresponding variation of Eq. (1) from the exact value for the same 15 cases was shown to be between 0.8% and 52.3%.

Having thus reposed faith in Eq. (2), expand the dimensional derivatives in terms of the nondimensional derivatives to obtain

$$\omega_p = \sqrt{\frac{g\left[C_{m_\alpha}\left(C_{L_u} + 2C_{L_1}\right) - \left(C_{m_u} + 2C_{m_1}\right)\left(C_{L_\alpha} + C_{D_1}\right)\right]}{\left(C_{m_q}\bar{c}/2\right)\left(C_{L_\alpha} + C_{D_1}\right) + (2m/\rho S)C_{m_\alpha}}} \tag{3}$$

The speed U_1 does not appear explicitly in the above equation, proving that the phugoid frequency is independent of the forward speed, provided the aerodynamic and thrust derivatives are held fixed by some means. This may be stated as an alternative conjecture.

Conjecture B. The phugoid frequency is independent of the forward speed, provided the aerodynamic and thrust derivatives are kept constant by some artificial means.

Although the approximate equation (2) is a fairly accurate representation of the phugoid frequency in the test cases of the recent study by the authors,[4] doubts still may persist over its validity when the speed is varied over a large band. Such fears are allayed by a provocative test in which both the approximate and the exact phugoid frequencies are calculated for a range of speeds varying from 50 to 1000 ft/s, far exceeding the flight envelopes of the aircraft in question. The approximate frequency is obtained by solving Eq. (2) and the exact value is obtained by solving the longitudinal characteristic equation

$$As^4 + Bs^3 + Cs^2 + Ds + E = 0 \tag{4}$$